

Universal V-shaped temperature-pressure phase diagram in the iron-based superconductors KFe_2As_2 , RbFe_2As_2 , and CsFe_2As_2

F. F. Tafti,^{1,*} A. Ouellet,¹ A. Juneau-Fecteau,¹ S. Faucher,¹ M. Lapointe-Major,¹ N. Doiron-Leyraud,¹ A. F. Wang,² X.-G. Luo,² X. H. Chen,² and Louis Taillefer^{3,4,†}

¹*Département de physique & RQMP, Université de Sherbrooke, Sherbrooke, Québec, Canada*

²*Hefei National Laboratory for Physical Sciences at Microscale and Department of Physics, University of Science and Technology of China, Hefei, China*

³*Département de physique & RQMP, Université de Sherbrooke, Sherbrooke, QC, Canada*

⁴*Canadian Institute for Advanced Research, Toronto, ON, Canada*

(Dated: April 23, 2022)

We report a sudden reversal in the pressure dependence of T_c in the iron-based superconductor RbFe_2As_2 , at a critical pressure $P_c = 11$ kbar. Combined with our prior results on KFe_2As_2 and CsFe_2As_2 , we find a universal V-shaped phase diagram for T_c vs P in these fully hole-doped 122 materials, when measured relative to the critical point (P_c, T_c) . From measurements of the upper critical field $H_{c2}(T)$ under pressure in KFe_2As_2 and RbFe_2As_2 , we observe the same two-fold jump in $(1/T_c)(-\partial H_{c2}/\partial T)_{T_c}$ across P_c , compelling evidence for a sudden change in the structure of the superconducting gap. We argue that this change is due to a transition from one pairing state to another, with different symmetries on either side of P_c . We discuss a possible link between scattering and pairing, and a scenario where a d -wave state favoured by high- Q scattering at low pressure changes to a state with s_{\pm} symmetry favoured by low- Q scattering at high pressure.

PACS numbers: 74.70.Xa, 74.62.Fj, 61.50.Ks

I. INTRODUCTION

Pairing symmetry in the iron based superconductors is controlled by the interband and the intraband interactions which are tunable by external parameters such as doping or pressure.^{1,2} Recent theoretical works using a five orbital tight binding model show a near degeneracy between d and s_{\pm} pairing states in the 122 iron pnictides as a result of the multiorbital structure of the Cooper pairs and the near nesting conditions.^{3,4} Hydrostatic pressure is a clean tuning parameter that can modify the orbital overlap, the exchange interactions, and the band structure of metals. Given the near degeneracy between different pairing states, it is conceivable that the pairing symmetry of certain iron-based superconductors can be tuned by pressure. These ideas gained experimental relevance with our recent discovery of a V-shaped T - P phase diagram in KFe_2As_2 and CsFe_2As_2 , where T_c decreases initially as a function of pressure, then at a critical pressure P_c , it suddenly changes direction and increases.^{5,6} Our results on KFe_2As_2 have been reproduced by other groups.⁷⁻⁹ We interpreted the transition at P_c as a change of pairing state, possibly from d to s_{\pm} , where the decreasing T_c of the former meets the growing T_c of the latter at P_c , resulting in a V-shaped phase diagram.

In this article, we present our discovery of a very similar V-shaped phase diagram in a third material: RbFe_2As_2 . We show that $\partial T_c/\partial P$ on both sides of P_c is the same in all three materials, which therefore share a universal V-shaped phase diagram. We show that the slope of $H_{c2}(T)$ jumps by a factor 2 across P_c , in a manner that also appears to be universal. This is compelling evidence for a sudden change in the gap structure,⁸ which

we attribute to a change of pairing symmetry.

The Fermi surface of KFe_2As_2 is known in detail from quantum oscillations studies.^{10,11} It consists of three quasi-2D hole-like cylinders centered on the Γ point, labelled α (small inner cylinder), ξ (middle cylinder), and β (large outer cylinder), as well as small cylindrical satellites at the corners of the Brillouin zone, labelled ε . There is also one small 3D hole pocket at the Z point of the Brillouin zone.¹² The pairing symmetry of KFe_2As_2 at ambient pressure is the subject of ongoing debate. Laser ARPES experiments suggest a s_{\pm} state with eight line nodes on the ξ band and no nodes on the α and β bands.^{13,14} By contrast, bulk measurements of thermal conductivity,^{15,16} heat capacity^{17,18} and penetration depth^{19,20} point to a d -wave state, with four line nodes on each of the Γ -centered Fermi pockets (α , ξ , and β).

II. METHODS

Single crystals of RbFe_2As_2 were grown using a self-flux method similar to KFe_2As_2 and CsFe_2As_2 .^{21,22} Two samples of RbFe_2As_2 , labelled Sample A and Sample B, were pressurized in a clamp cell and measured up to 22 kbar. The pressure was measured by monitoring the superconducting transition of a lead gauge placed besides the two samples in the clamp cell with a precision of ± 0.1 kbar. A 1/1 mixture of pentane and 3-methyl-1-butanol was used as the pressure medium. Measurements of resistivity and Hall effect were performed on both samples in an adiabatic demagnetization refrigerator using the standard six-contact configuration. Hall voltage was measured at plus and minus 10 T from $T = 20$ to 1 K

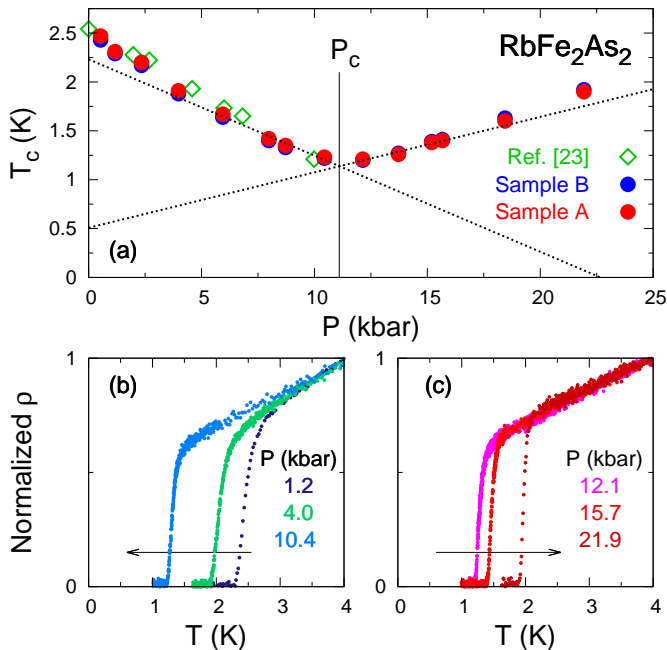


FIG. 1. (a) Pressure dependence of T_c in RbFe_2As_2 . The red and blue circles represent data from Samples A and B, respectively. T_c is defined as the temperature where $\rho = 0$. The critical pressure P_c marks the reversal in the T_c behaviour from decreasing to increasing. Dotted lines are linear fits to the data in the range $P_c \pm 6$ kbar. The critical pressure $P_c = 11 \pm 1$ kbar is defined as the intersection of the two dotted lines. The green diamonds are data from Ref. [23], where T_c was measured by AC susceptibility and μSR . (b) Three representative $\rho(T)$ curves in the low pressure phase ($P < P_c$), from Sample A, normalized to unity at $T = 4$ K. The arrow shows that T_c decreases with increasing pressure. (c) Same as in (b) for the high pressure phase ($P > P_c$). The arrow shows that T_c now *increases* with increasing pressure.

and antisymmetrized to calculate the Hall coefficient R_H . Excellent reproducibility was observed between the two samples. To avoid redundancy, we present the results from Sample A, unless otherwise mentioned.

III. RESULTS AND DISCUSSION

We have measured the pressure dependence of four quantities: the critical temperature T_c , the Hall coefficient R_H , the upper critical field $H_{c2}(T)$, and the resistivity ρ . We present each measurement in turn, and discuss the implications.

A. Pressure dependence of T_c

Figure 1(a) shows our discovery of a sudden reversal in the pressure dependence of T_c in RbFe_2As_2 at a critical pressure $P_c = 11 \pm 1$ kbar. On the same figure,

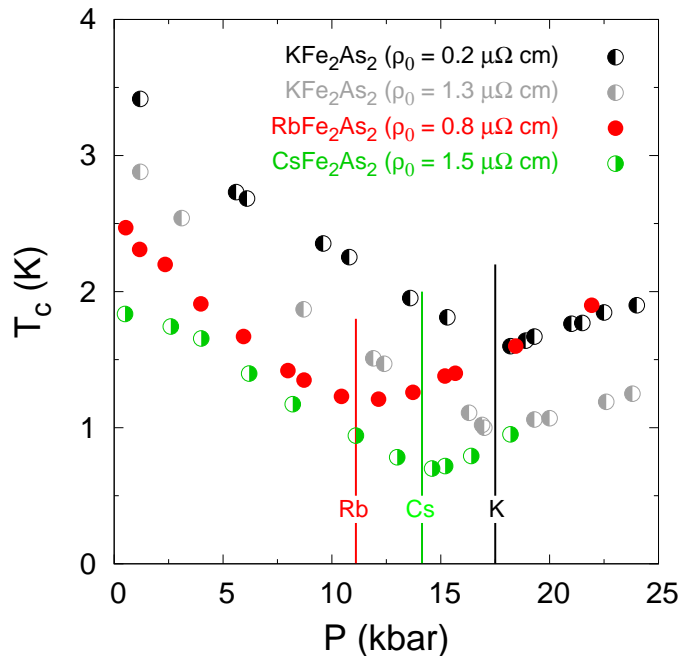


FIG. 2. Temperature-pressure phase diagram of KFe_2As_2 (black and grey), RbFe_2As_2 (red), and CsFe_2As_2 (green). The residual resistivity ρ_0 of each sample is indicated. Comparing the black and grey points shows that P_c is unaffected by disorder. The three compounds show a T_c reversal at comparable critical pressures (color-coded vertical lines): $P_c = 17.5$, 11, and 14 kbar, in KFe_2As_2 , RbFe_2As_2 and CsFe_2As_2 , respectively. Data for KFe_2As_2 and CsFe_2As_2 are reproduced from Refs. 5 and 6, respectively. Error bars are no larger than the size of the points.

the green diamonds show T_c values reported previously for RbFe_2As_2 from AC susceptibility and μSR measurements up to 10 kbar by Shermadini *et al.*²³ These data are in excellent agreement with ours, but they stop at 10 kbar, just before P_c . By extrapolation, Shermadini *et al.* concluded that T_c would be fully suppressed at 19 kbar which is the natural expectation from a superconductor with one dominant pairing state.

We determined T_c from resistivity measurements using a $\rho = 0$ criterion. Figure 1(b) shows three representative resistivity curves at $P < P_c$, where T_c decreases by increasing pressure. Figure 1(c) shows three curves at $P > P_c$, where T_c reverses direction to increase by increasing pressure. T_c varies linearly near P_c from either side, resulting in a V-shaped phase diagram in RbFe_2As_2 , similar to KFe_2As_2 and CsFe_2As_2 .^{5,6}

In Fig. 2, we compare the phase diagrams of KFe_2As_2 , RbFe_2As_2 and CsFe_2As_2 , with $P_c = 17.5$, 11, and 14 kbar, respectively. The black and grey symbols correspond to two samples of KFe_2As_2 with different disorder levels. Although the residual resistivity of the less pure sample ($\rho_0 = 1.3 \mu\Omega \text{ cm}$) is six times larger than that of the pure sample ($\rho_0 = 0.2 \mu\Omega \text{ cm}$), they have identical P_c . Hence, disorder does not affect the critical pressure.

TABLE I. Lattice parameters (a and c), unit cell volume ($V = ca^2$), Sommerfeld coefficient in the specific heat (γ), critical temperature T_c at ambient pressure, T_c at P_c , and critical pressure P_c , for KFe_2As_2 , RbFe_2As_2 and CsFe_2As_2 .^{21,22,24–26} As the atomic size of the alkali ion increases from K to Rb to Cs, lattice parameters, unit cell volume, and the Sommerfeld coefficient systematically increase, while T_c systematically decreases. But the critical pressure P_c does not follow these systematics: it decreases from K to Rb, then increases from Rb to Cs.

Material	a (Å)	c (Å)	V (Å ³)	γ (mJ/K ² mol)	T_c ($P = 0$) (K)	T_c ($P = P_c$) (K)	P_c (kbar)
KFe_2As_2	3.84	13.84	204	99	3.6	1.6	17.5
RbFe_2As_2	3.86	14.45	215	128	2.5	1.2	11
CsFe_2As_2	3.89	15.07	228	184	1.8	0.7	14

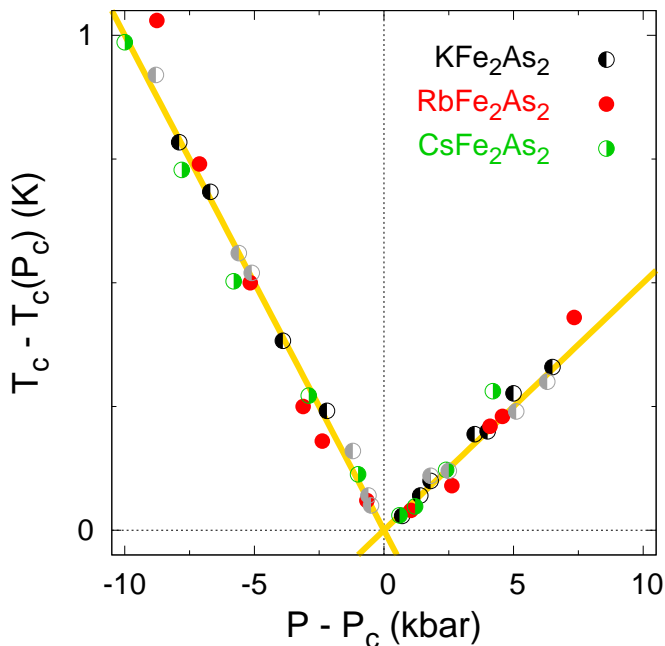


FIG. 3. Universal V-shaped phase diagram of AFe_2As_2 , where $A = \text{K}$ (black and grey), Rb (red) and Cs (green). Data points from Fig. 2 are re-plotted with pressure values shifted by the respective critical pressures ($P_c = 17.5$, 11, and 14 kbar, for $A = \text{K}$, Rb , and Cs) and T_c values shifted by the respective values of T_c at P_c (1.6, 1.2, and 0.7 K, for $A = \text{K}$, Rb , and Cs). Error bars are no larger than the size of the points. The yellow lines are linear fits on either side of P_c .

Figure 2 also shows that the phase diagram of the less pure KFe_2As_2 sample (gray) is rigidly shifted down relative to the pure sample (black). Therefore, the low-pressure and the high-pressure superconducting phases have comparable (and large) sensitivity to disorder. The high sensitivity to disorder on both sides of P_c is incompatible with the standard s_{++} state, known to be resilient against disorder.^{27,28} In KFe_2As_2 at ambient pressure, the steep drop of T_c as a function of controlled disorder was shown to be quantitatively consistent with the high sensitivity of a d -wave state to disorder.^{15,29,30} Since the usual s_{\pm} state, with a sign change between pockets centered at different points in the Brillouin zone, is known to be much less sensitive to disorder than the d -wave

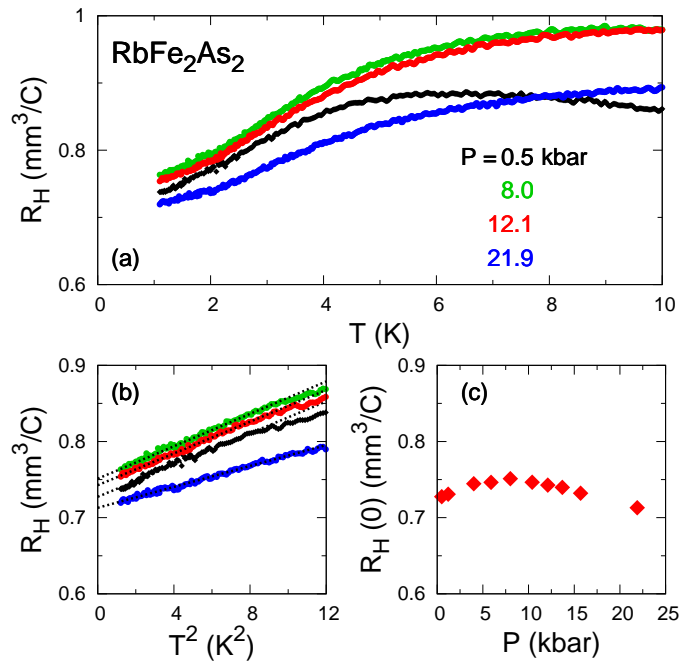


FIG. 4. (a) Temperature dependence of the Hall coefficient $R_H(T)$ in RbFe_2As_2 at four pressures as indicated. (b) $R_H(T)$ plotted versus T^2 for the same pressures as in (a), at low temperature. The dotted lines are linear fits from which the zero-temperature limit of the Hall coefficient, $R_H(0)$, is obtained at each pressure. (c) $R_H(0)$ plotted as a function of pressure, showing a small but smooth variation. Vertical and horizontal error bars are no larger than the size of the points. Vertical error bars come from the uncertainty in the T^2 fits in (b), associated with changing the fitting interval.

state,³⁰ it may be that the high pressure phase is the s_{\pm}^h state proposed for KFe_2As_2 ,³¹ where the gap changes sign between two of the Γ -centered pockets resulting in a higher sensitivity to disorder.

By measuring the lattice parameters of KFe_2As_2 under pressure, we showed in Ref. [6] that it takes about 30 kbar to tune the unit cell volume and the As-Fe-As bond angle of CsFe_2As_2 to match those of KFe_2As_2 . Therefore, if the structural parameters directly controlled P_c , one would expect the critical pressure of CsFe_2As_2 to be 30 kbar larger than that of KFe_2As_2 . As shown in Fig. 2, the P_c of CsFe_2As_2 is *less* than the P_c of KFe_2As_2 . Table I lists the

structural parameters of the three compounds at ambient pressure. Rb atoms are intermediate in size between K and Cs, hence the lattice parameters of RbFe_2As_2 are in between those of KFe_2As_2 and CsFe_2As_2 . Fig. 2 shows that the P_c of RbFe_2As_2 does not fall between those of the other two compounds. There is indeed no straightforward connection between lattice parameters, bond angles, or ionic sizes and the actual values of P_c in these three compounds. Interestingly, near optimal doping, in both 122 and 1111 families, there *is* indeed a straightforward connection between the structural parameters and T_c .^{32,33} Near optimal doping, d wave is known to be a subdominant superconducting state while s wave is the dominant one.³⁴ The Loss of this straightforward connection between superconductivity and structural parameters in the over-doped regime could in fact result from a dominant d wave state.

In Fig. 3, we make a direct comparison of the three V-shaped phase diagrams, by shifting each curve horizontally by P_c and vertically by $T_c(P=P_c)$, so that the tip of the V coincides for the three materials. Remarkably, we find the same, universal V-shaped phase diagram in the range $P_c \pm 10$ kbar. In other words, $(\partial T_c/\partial P)_{P < P_c}$ and $(\partial T_c/\partial P)_{P > P_c}$ are identical in the three materials. Such a universal phase diagram, independent of the alkali atom (A) in AFe_2As_2 and of the different structural parameters, poses a clear challenge to our understanding of multiband superconductivity.

B. Pressure dependence of R_H

In our previous work on KFe_2As_2 and CsFe_2As_2 , we showed that the V-shaped pressure dependence of T_c is not accompanied by any abrupt changes in the normal-state properties. In particular, the zero-temperature limit of the Hall coefficient, $R_H(0)$, was found constant in both materials as a function of pressure across P_c , ruling out a sudden change in the Fermi surface, i.e. a Lifshitz transition.^{5,6} We concluded that the phase transition at P_c is not triggered by some change in the Fermi surface, and is instead associated with a change in the superconducting state itself. This was confirmed by quantum oscillation measurements on KFe_2As_2 under pressure, which found a smooth evolution of the oscillation frequencies and cyclotron masses across P_c .⁷

Figure 4(a) shows the temperature dependence of R_H in RbFe_2As_2 , at various pressures. The low-temperature data goes as T^2 , allowing us to extract $R_H(0)$ from a linear fit of $R_H(T)$ vs T^2 , as shown in Fig. 4(b). The $R_H(0)$ values are plotted as a function of pressure in Fig. 4(c). We find a small but smooth variation in $R_H(0)$, with no anomaly at $P_c = 11$ kbar, very different from the step-like structure expected of a typical Lifshitz transition.³⁵

In Figure 5, we summarize the results of our Hall measurements in the three materials. In KFe_2As_2 and CsFe_2As_2 , $R_H(0)$ is completely flat with pressure. In

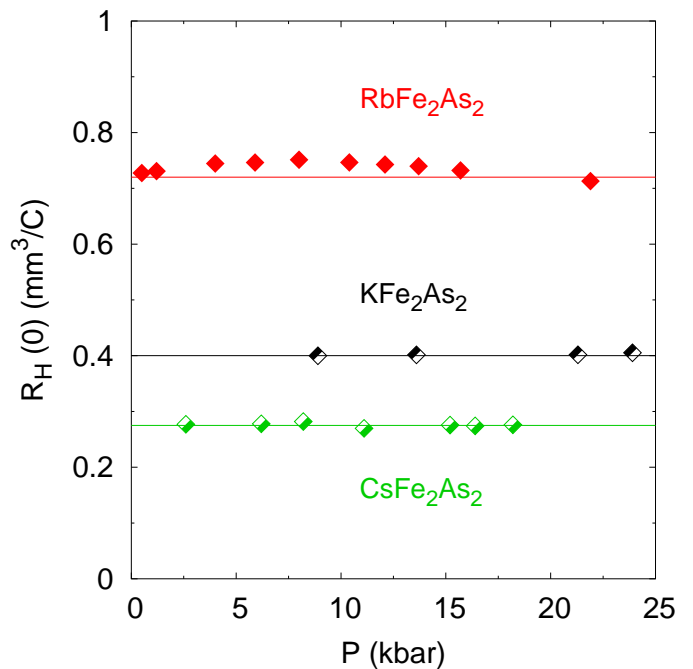


FIG. 5. The zero-temperature limit of the Hall coefficient, $R_H(0)$, plotted for the three materials AFe_2As_2 , where A = K (black), Rb (red), and Cs (green). Vertical and horizontal error bars are no larger than the size of the points. Within error bars, $R_H(0)$ is constant for KFe_2As_2 and CsFe_2As_2 , and nearly so for RbFe_2As_2 . Horizontal lines are a guide to the eye. Data for KFe_2As_2 and CsFe_2As_2 are reproduced from Refs. 5 and 6, respectively.

RbFe_2As_2 , there is a broad structure in $R_H(0)$ and a straight line does not go through all data points. We attribute this broad feature to a smooth evolution of Fermi surface parameters under pressure. Taken together, these Hall data make a compelling case that the universal V-shaped T_c vs P curve of Fig. 3 is not shaped by a sudden change in the Fermi surface at P_c .

C. Pressure dependence of H_{c2}

Measurements of the upper critical field H_{c2} in KFe_2As_2 under pressure can be used to provide evidence for a change of gap structure across P_c . Recently, Taufour *et al.* found a change of regime in the dependence of the quantity $(1/T_c)(-\partial H_{c2}/\partial T)_{T_c}$ as a function of the A coefficient of resistivity from $\rho(T) = \rho_0 + AT^2$.⁸ They linked this change of regime to a change in the k_z corrugations of the superconducting gap at the critical pressure P_c . Inspired by their work, we explored the pressure dependence of H_{c2} in both KFe_2As_2 and RbFe_2As_2 .

At any given pressure, we used measurements of $\rho(T)$ at different fields to determine $H_{c2}(T)$. Figure 6 shows normalized $\rho(T)$ curves in RbFe_2As_2 at different fields, for four representative pressures, below and above $P_c = 11$ kbar. We define T_c at each field from the resis-

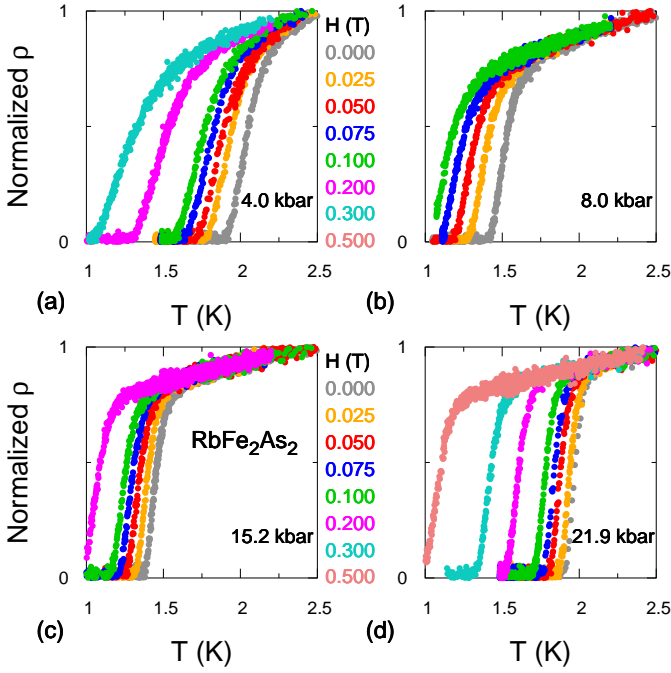


FIG. 6. Resistivity $\rho(T)$ of RbFe_2As_2 normalized to unity at $T = 2.5$ K, at $P = 4.0, 8.0, 15.2,$ and 21.9 kbar. The color of each curve corresponds to a field H as indicated. At each field, T_c is defined from the resistive transition using the criterion $\rho = 0$. This yields the curves of H_{c2} vs T in Fig. 7(a). Note that the width of the transition is larger in the low-pressure phase (e.g. in (a)) compared to the high-pressure phase (e.g. in (d)), because $\partial T_c / \partial P$ is almost two times higher in the low-pressure phase (Fig. 3). Therefore, a small pressure gradient across the sample in the pressure cell generates a wider transition in the low-pressure phase.

tive transition using the $\rho = 0$ criterion, then plot those T_c values vs H at each pressure, to arrive at the H - T curves shown in Fig. 7(a).

The four $H_{c2}(T)$ curves in Fig. 7(a) should be viewed in two pairs with comparable T_c values on either side of P_c , as illustrated in Fig. 7(b). Figure 7(c) summarizes the results by plotting $(-\partial H_{c2} / \partial T)_{T_c}$ versus T_c for the two pairs of points at $T_c = 1.4$ K and 1.9 K. At each value of T_c , the full symbol lies above the empty one, showing that the high-pressure phase is more robust against the magnetic field than the low-pressure phase. To obtain $(-\partial H_{c2} / \partial T)_{T_c}$ in RbFe_2As_2 , we made linear fits to the H - T curves in Fig. 7(a) near T_c .

Figure 8 shows $(1/T_c)(-\partial H_{c2} / \partial T)_{T_c}$ vs $(P - P_c)$ for both RbFe_2As_2 and KFe_2As_2 . In total, we measured $H_{c2}(T)$ at six different pressures, corresponding to the six red squares in Fig. 8. The four black data points in Fig. 8 come from similar measurements on KFe_2As_2 , from the $H_{c2}(T)$ curves shown in Fig. 9. The magnitude of $(1/T_c)(-\partial H_{c2} / \partial T)_{T_c}$ is the same in the two materials, on both sides of P_c , revealing a second universal property of the pressure-induced transition: a two-fold jump in $(1/T_c)(-\partial H_{c2} / \partial T)_{T_c}$ at $P = P_c$ (Fig. 8).

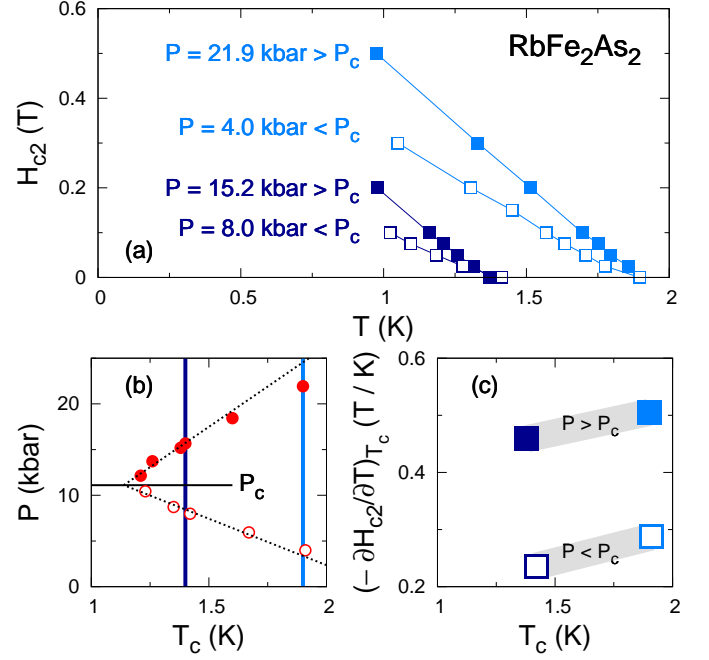


FIG. 7. The full symbols in this figure represent the high-pressure phase ($P > P_c$) and the empty symbols represent the low-pressure phase ($P < P_c$). (a) $H_{c2}(T)$ in RbFe_2As_2 at four pressures. The light blue pair of curves starts from $T_c \simeq 1.9$ K and the dark blue pair starts from $T_c \simeq 1.4$ K, at $H = 0$. At a given T_c , the low pressure curve has a lower slope compared to the high pressure one. (b) The V-shape phase diagram of RbFe_2As_2 , rotated by 90 degrees, with lines that cut through the “V” at pairs of pressures corresponding to the light blue and the dark blue curves in panel (a). (c) $(-\partial H_{c2} / \partial T)_{T_c}$ is extracted from linear fits to the curves in panel (a) near T_c and plotted against T_c . The light blue pair of points is vertically aligned at $T_c \simeq 1.9$ K and the dark blue pair at $T_c \simeq 1.4$ K corresponding to the vertical lines in panel (b). Error bars are no larger than the size of the points. We observe that consistently, $(-\partial H_{c2} / \partial T)_{T_c}$ is larger in the high pressure phase.

The Helfand-Werthamer theory, modified for superconductors with anisotropic gap structures,³⁶ relates the quantity $(1/T_c)(-\partial H_{c2} / \partial T)_{T_c}$ to the gap dispersion Ω and the anisotropic Fermi velocity v_0 through the relation:

$$\frac{1}{T_c} \left(\frac{-\partial H_{c2}}{\partial T} \right)_{T_c} = \frac{16\pi\phi_0 k_B^2}{7\zeta(3)\hbar^2} \frac{1}{\langle \Omega^2 \mu_c \rangle} \frac{1}{v_0^2} \quad (1)$$

where ϕ_0 , \hbar , and k_B are the magnetic flux quantum, the Planck constant, and the Boltzmann constant. μ_c and v_0 relate to the Fermi surface parameters according to:

$$\mu_c = \frac{v_x^2 + v_y^2}{v_0^2} \quad \text{and} \quad v_0^3 = \frac{2E_F^2}{\pi^2 \hbar^3 N(0)} \quad (2)$$

Where E_F and $N(0)$ are the Fermi energy and the density of states at the Fermi level. Fermi velocity is not a constant at anisotropic Fermi surfaces, hence, a char-

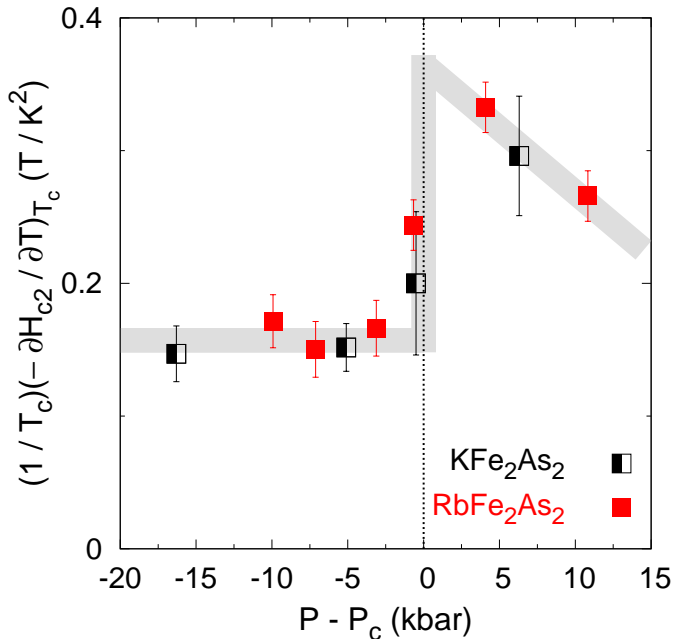


FIG. 8. $(1/T_c)(-\partial H_{c2}/\partial T)_{T_c}$ as a function of $P - P_c$ in RbFe_2As_2 (red squares) and KFe_2As_2 (black squares). The two materials are seen to display the same behaviour, with the same magnitude on both sides of P_c . The thick gray line is a guide to the eye. A two-fold jump is observed at $P = P_c$, revealing a clear difference between the low-pressure phase ($P - P_c < 0$) and the high-pressure phase ($P - P_c > 0$).

acteristic constant velocity v_0 is defined in Eq. 2 applicable to anisotropic Fermi surfaces.³⁶ For the isotropic case, one recovers $v_0 = v_F$. The function Ω describes the momentum dependence of the superconducting gap: $\Delta = \Psi(\mathbf{r}, \mathbf{T})\Omega(\mathbf{k}_F)$. The averages $\langle \dots \rangle$ are taken over the Fermi surface.

Given that quantum oscillation measurements in KFe_2As_2 under pressure show a smooth evolution of v_F across P_c ,⁷ the two-fold jump in $(1/T_c)(-\partial H_{c2}/\partial T)_{T_c}$ observed at P_c can only be the result of a sudden change in the gap dispersion function Ω in Eq. 1, caused by a sudden change in the structure of the superconducting gap across P_c . The most natural mechanism for such a change is a transition from one pairing state to another, with a change of symmetry, *e.g.* from d -wave to s -wave.

D. Pressure dependence of $\rho(T)$

In a recent theoretical work, Fernandes and Millis showed how different spin-mediated pairing interactions in iron-based superconductors can favor different pairing symmetries.⁴ In their model, based on the standard Fermi surface with hole-like pockets at the Γ point and electron pockets at the X points, SDW-type magnetic fluctuations, with wavevector $(\pi, 0)$, favour s_{\pm} pairing, whereas Néel-type fluctuations, with wavevector (π, π) ,

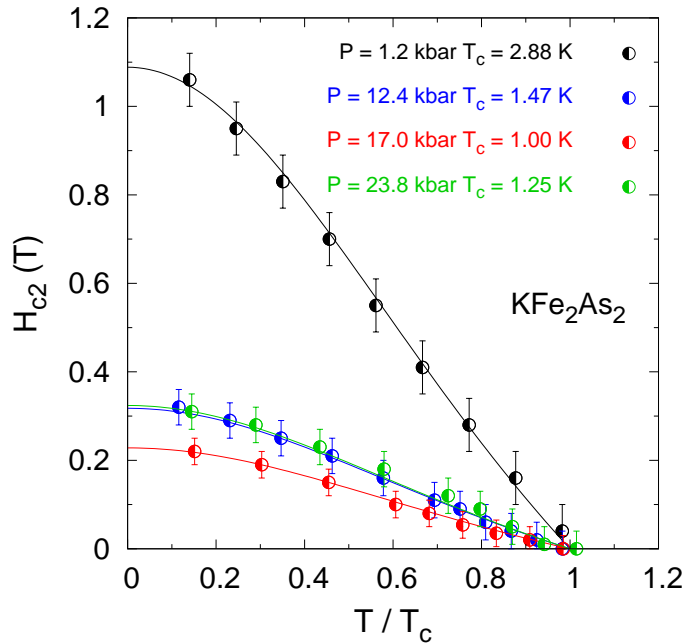


FIG. 9. $H_{c2}(T)$ in KFe_2As_2 plotted as a function of T/T_c . At each pressure, $(-\partial H_{c2}/\partial T)_{T_c}$ is obtained by fitting a line to the $H_{c2}(T)$ curve near T_c . The resulting $(1/T_c)(-\partial H_{c2}/\partial T)_{T_c}$ values are the black data points in Fig. 8. Solid lines are a guide to the eye.

favour d -wave pairing. A gradual increase in the (π, π) fluctuations rapidly suppresses the s_{\pm} superconducting state and eventually causes a phase transition from the s_{\pm} state to a d -wave state, producing a V-shaped phase diagram of T_c vs tuning parameter (strength of (π, π) correlations).⁴

It is conceivable that two such competing interactions are at play in AFe_2As_2 , with pressure tilting the balance in favor of one versus the other. We explore such a scenario by looking at how the inelastic scattering evolves with pressure, measured via the inelastic resistivity, defined as $\rho(T = 20\text{K}) - \rho_0$. Figure 10 shows the temperature dependence of resistivity, at six representative pressures, in RbFe_2As_2 . The residual resistivity ρ_0 comes from a power-law fit to the resistivity at any pressure, of the form $\rho = \rho_0 + AT^n$. The resulting ρ_0 does not change with pressure. $\rho(T = 20\text{K})$ is the value of the resistivity at $T = 20$ K, at any given pressure. Through the same procedure, we extracted ρ_0 and $\rho(T = 20\text{K})$ as a function of pressure in KFe_2As_2 and CsFe_2As_2 , from published data.^{5,6} In Fig. 11, the inelastic resistivity $\rho(T = 20\text{K}) - \rho_0$ is plotted as a function of $P - P_c$. In all three materials, at $P - P_c > 0$, the inelastic resistivity varies linearly with pressure. As P drops below P_c in the low pressure phase ($P - P_c < 0$), the inelastic resistivity shows a clear rise over and above the linear regime. Figure 11 therefore suggests a connection between the transition in the pressure dependence of T_c and the appearance of an additional inelastic scatter-

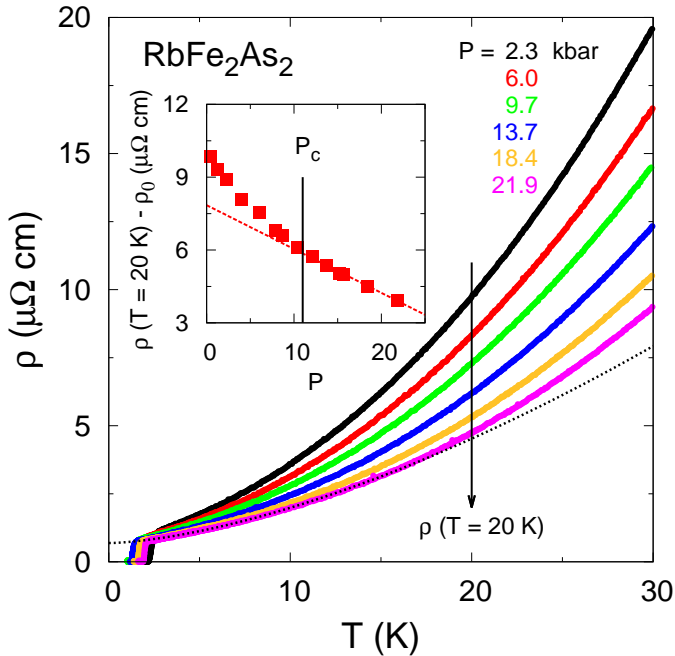


FIG. 10. Resistivity of sample A as a function of temperature up to 30 K, at six representative pressures, as indicated. The vertical arrow that cuts through the resistivity curves at $T = 20$ K defines $\rho(T = 20\text{K})$. The black dotted line is a power law fit to the resistivity curve at $P = 21.9$ kbar, in the interval from $T = 3$ K to 15 K. We define the residual resistivity ρ_0 as the zero temperature limiting value of this fit. The inset shows the pressure dependence of the inelastic resistivity, $\rho(T = 20\text{K}) - \rho_0$. The vertical arrow in the inset shows $P_c = 11$ kbar. The red dashed line is a linear fit to the inelastic resistivity as a function of pressure at $P > P_c$.

ing channel. Note that our choice of $T = 20$ K to define the inelastic resistivity is arbitrary; resistivity cuts at any other temperature above T_c give qualitatively similar results.

Now, the intraband inelastic scattering wavevectors that favour d -wave pairing in KFe_2As_2 are large- Q processes where Q is the momentum transfer.³⁷ By contrast, theoretical calculations show that the s_{\pm}^h pairing state, which changes sign between the α and the ξ hole pockets, is favoured by small- Q interband interactions.³¹ Therefore, one scenario in which to understand the evolution in the inelastic resistivity with pressure (Fig. 11), and its link to the T_c reversal, is the following. At low pressure, the large- Q scattering processes that favor d -wave pairing make a substantial contribution to the resistivity, as they produce a large change in momentum. These weaken with pressure, causing a decrease in both T_c and the resistivity. This decrease persists until the low- Q processes that favor s_{\pm}^h pairing, less visible in the resistivity, come to dominate, above P_c .

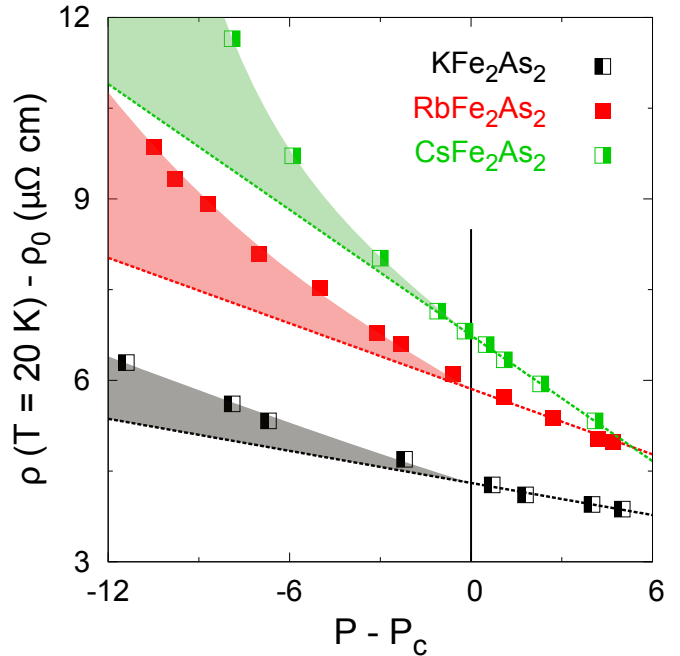


FIG. 11. Inelastic resistivity defined as $\rho(T = 20\text{K}) - \rho_0$ and plotted versus $P - P_c$ in KFe_2As_2 (black symbols, $P_c = 17.5$ kbar), RbFe_2As_2 (red symbols, $P_c = 11$ kbar), and CsFe_2As_2 (green symbols, $P_c = 14$ kbar). Dashed lines are linear fits to the data at $P - P_c > 0$ showing that the inelastic resistivity scales linearly with pressure in the high pressure phase above P_c . As the pressure is lowered below P_c , a new channel contributes to the inelastic resistivity of AFe_2As_2 shown as shaded areas in gray, red, and green for $A = \text{K}, \text{Rb},$ and Cs . The vertical black line marks $P = P_c$.

IV. SUMMARY

In summary, we report a universal V-shaped pressure dependence of T_c in AFe_2As_2 with $A = \text{K}, \text{Rb},$ and Cs . Remarkably, the temperature-pressure superconducting phase diagram of these fully hole-doped iron arsenides is universal, unaffected by a change in the alkali atom A , with its concomitant changes in structural parameters. In the absence of any sudden change in the Fermi surface across the critical pressure P_c , we interpret the T_c reversal at P_c as a transition from one pairing state to another. The observation of a sudden change in the upper critical field $H_{c2}(T)$, which also appears to be universal in that it is identical in RbFe_2As_2 and KFe_2As_2 , is compelling evidence of a sudden change in the structure of the superconducting gap across P_c . Our proposal is a d -wave state below P_c and a so-called s_{\pm}^h state, where the gap changes sign between Γ -centered hole pockets, above P_c . Our study of the pressure dependence of resistivity in KFe_2As_2 , CsFe_2As_2 , and RbFe_2As_2 reveals a possible link between T_c and inelastic scattering. As the pressure is lowered, the large- Q inelastic scattering processes that favour d -wave pairing grow until at a critical pressure P_c they cause a change of pairing symmetry from s -wave

to d -wave.

ACKNOWLEDGMENTS

We thank J. Carbotte, A. V. Chubukov, J. P. Clancy, R. M. Fernandes, M. Franz, Y.-J. Kim, C. Meingast, A. J. Millis, R. Prozorov, P. Richard, M. A. Tanatar, V. Taufour, I. Vekhter, and H. von Löhneysen for helpful

discussions, as well as B. Vincent and S. Fortier for assistance with the experiments. The work at Sherbrooke was supported by the Canadian Institute for Advanced Research and a Canada Research Chair and it was funded by NSERC, FRQNT and CFI. Work done in China was supported by the National Natural Science Foundation of China (Grant No. 11190021), the Strategic Priority Research Program (B) of the Chinese Academy of Sciences, and the National Basic Research Program of China.

-
- * Fazel.Fallah.Tafti@USherbrooke.ca
 † Louis.Taillefer@USherbrooke.ca
- ¹ A. Chubukov, Annual Review of Condensed Matter Physics **3**, 57 (2012).
 - ² P. J. Hirschfeld, M. M. Korshunov, and I. I. Mazin, Reports on Progress in Physics **74**, 124508 (2011).
 - ³ S. Graser, T. A. Maier, P. J. Hirschfeld, and D. J. Scalapino, New Journal of Physics **11**, 025016 (2009).
 - ⁴ R. M. Fernandes and A. J. Millis, Physical Review Letters **110**, 117004 (2013).
 - ⁵ F. F. Tafti, A. Juneau-Fecteau, M.-E. Delage, S. René de Cotret, J.-P. Reid, A. F. Wang, X.-G. Luo, X. H. Chen, N. Doiron-Leyraud, and L. Taillefer, Nature Physics **9**, 349 (2013).
 - ⁶ F. F. Tafti, J. P. Clancy, M. Lapointe-Major, C. Collignon, S. Faucher, J. A. Sears, A. Juneau-Fecteau, N. Doiron-Leyraud, A. F. Wang, X.-G. Luo, X. H. Chen, S. Desgreniers, Y.-J. Kim, and L. Taillefer, Physical Review B **89**, 134502 (2014).
 - ⁷ T. Terashima, K. Kihou, K. Sugii, N. Kikugawa, T. Matsumoto, S. Ishida, C.-H. Lee, A. Iyo, H. Eisaki, and S. Uji, Physical Review B **89**, 134520 (2014).
 - ⁸ V. Taufour, N. Foroozani, M. A. Tanatar, J. Lim, U. Kaluarachchi, S. K. Kim, Y. Liu, T. A. Lograsso, V. G. Kogan, R. Prozorov, S. L. Bud'ko, J. S. Schilling, and P. C. Canfield, Physical Review B **89**, 220509 (2014).
 - ⁹ V. Grinenko, W. Schottenhamel, A. U. B. Wolter, D. V. Efremov, S.-L. Drechsler, S. Aswartham, M. Kumar, S. Wurmehl, M. Roslova, I. V. Morozov, B. Holzapfel, B. Büchner, E. Ahrens, S. I. Troyanov, S. Köhler, E. Gati, S. Knöner, N. H. Hoang, M. Lang, F. Ricci, and G. Profeta, Physical Review B **90**, 094511 (2014).
 - ¹⁰ T. Terashima, M. Kimata, N. Kurita, H. Satsukawa, A. Harada, K. Hazama, M. Imai, A. Sato, K. Kihou, C.-H. Lee, H. Kito, H. Eisaki, A. Iyo, T. Saito, H. Fukazawa, Y. Kohori, H. Harima, and S. Uji, Journal of the Physical Society of Japan **79**, 053702 (2010).
 - ¹¹ T. Terashima, N. Kurita, M. Kimata, M. Tomita, S. Tsuchiya, M. Imai, A. Sato, K. Kihou, C.-H. Lee, H. Kito, H. Eisaki, A. Iyo, T. Saito, H. Fukazawa, Y. Kohori, H. Harima, and S. Uji, Physical Review B **87**, 224512 (2013).
 - ¹² Diego A. Zocco, Kai Grube, Felix Eilers, Thomas Wolf, and Hilbert v. Löhneysen, in *Proceedings of the International Conference on Strongly Correlated Electron Systems*, JPS Conference Proceedings, Vol. 3 (Journal of the Physical Society of Japan, 2014) p. 015007.
 - ¹³ K. Okazaki, Y. Ota, Y. Kotani, W. Malaeb, Y. Ishida, T. Shimojima, T. Kiss, S. Watanabe, C.-T. Chen, K. Kihou, C. H. Lee, A. Iyo, H. Eisaki, T. Saito, H. Fukazawa, Y. Kohori, K. Hashimoto, T. Shibauchi, Y. Matsuda, H. Ikeda, H. Miyahara, R. Arita, A. Chainani, and S. Shin, Science **337**, 1314 (2012).
 - ¹⁴ D. Watanabe, T. Yamashita, Y. Kawamoto, S. Kurata, Y. Mizukami, T. Ohta, S. Kasahara, M. Yamashita, T. Saito, H. Fukazawa, Y. Kohori, S. Ishida, K. Kihou, C. H. Lee, A. Iyo, H. Eisaki, A. B. Vorontsov, T. Shibauchi, and Y. Matsuda, Physical Review B **89**, 115112 (2014).
 - ¹⁵ J.-P. Reid, M. A. Tanatar, A. Juneau-Fecteau, R. T. Gordon, S. René de Cotret, N. Doiron-Leyraud, T. Seito, H. Fukazawa, Y. Kohori, K. Kihou, C. H. Lee, A. Iyo, H. Eisaki, R. Prozorov, and L. Taillefer, Physical Review Letters **109**, 087001 (2012).
 - ¹⁶ J.-P. Reid, A. Juneau-Fecteau, R. T. Gordon, S. René de Cotret, N. Doiron-Leyraud, X.-G. Luo, H. Shakeripour, J. Chang, M. A. Tanatar, H. Kim, R. Prozorov, T. Saito, H. Fukazawa, Y. Kohori, K. Kihou, C. H. Lee, A. Iyo, H. Eisaki, B. Shen, H.-H. Wen, and L. Taillefer, Superconductor Science and Technology **25**, 084013 (2012).
 - ¹⁷ M. Abdel-Hafiez, V. Grinenko, S. Aswartham, I. Morozov, M. Roslova, O. Vakaliuk, S. Johnston, D. V. Efremov, J. van den Brink, H. Rosner, M. Kumar, C. Hess, S. Wurmehl, A. U. B. Wolter, B. Büchner, E. L. Green, J. Wosnitza, P. Vogt, A. Reifenberger, C. Enss, M. Hempel, R. Klingeler, and S.-L. Drechsler, Physical Review B **87**, 180507 (2013).
 - ¹⁸ V. Grinenko, D. V. Efremov, S.-L. Drechsler, S. Aswartham, D. Gruner, M. Roslova, I. Morozov, K. Nenkov, S. Wurmehl, A. U. B. Wolter, B. Holzapfel, and B. Büchner, Physical Review B **89**, 060504 (2014).
 - ¹⁹ K. Hashimoto, A. Serafin, S. Tonegawa, R. Katsumata, R. Okazaki, T. Saito, H. Fukazawa, Y. Kohori, K. Kihou, C. H. Lee, A. Iyo, H. Eisaki, H. Ikeda, Y. Matsuda, A. Carrington, and T. Shibauchi, Physical Review B **82**, 014526 (2010).
 - ²⁰ H. Kim, M. A. Tanatar, Y. Liu, Z. C. Sims, C. Zhang, P. Dai, T. A. Lograsso, and R. Prozorov, Physical Review B **89**, 174519 (2014).
 - ²¹ A. F. Wang, B. Y. Pan, X. G. Luo, F. Chen, Y. J. Yan, J. J. Ying, G. J. Ye, P. Cheng, X. C. Hong, S. Y. Li, and X. H. Chen, Physical Review B **87**, 214509 (2013).
 - ²² Z. Zhang, A. F. Wang, X. C. Hong, J. Zhang, B. Y. Pan, J. Pan, Y. Xu, X. G. Luo, X. H. Chen, and S. Y. Li, arXiv:1403.0191 (2014).
 - ²³ Z. Shermadini, H. Luetkens, A. Maisuradze, R. Khasanov, Z. Bukowski, H.-H. Klauss, and A. Amato, Physical Review B **86**, 174516 (2012).
 - ²⁴ K. Sasmal, B. Lv, B. Lorenz, A. M. Guloy, F. Chen, Y.-Y. Xue, and C.-W. Chu, Physical Review Letters **101**, 107007 (2008).

- ²⁵ M. Aftabuzzaman and A. K. M. A. Islam, *Physica C: Superconductivity* **470**, 202 (2010).
- ²⁶ F. Hardy, A. E. Böhmer, D. Aoki, P. Burger, T. Wolf, P. Schweiss, R. Heid, P. Adelman, Y. X. Yao, G. Kotliar, J. Schmalian, and C. Meingast, *Physical Review Letters* **111**, 027002 (2013).
- ²⁷ P. W. Anderson, *Journal of Physics and Chemistry of Solids* **11**, 26 (1959).
- ²⁸ R. Prozorov, M. Konczykowski, M. A. Tanatar, A. Thaler, S. L. Budko, P. C. Canfield, V. Mishra, and P. J. Hirschfeld, *Physical Review X* **4**, 041032 (2014).
- ²⁹ A. F. Wang, S. Y. Zhou, X. G. Luo, X. C. Hong, Y. J. Yan, J. J. Ying, P. Cheng, G. J. Ye, Z. J. Xiang, S. Y. Li, and X. H. Chen, *Physical Review B* **89**, 064510 (2014).
- ³⁰ K. Kirshenbaum, S. R. Saha, S. Ziemak, T. Drye, and J. Paglione, *Physical Review B* **86**, 140505 (2012).
- ³¹ S. Maiti, M. M. Korshunov, and A. V. Chubukov, *Physical Review B* **85**, 014511 (2012).
- ³² M. Rotter, M. Pangerl, M. Tegel, and D. Johrendt, *Angewandte Chemie International Edition* **47**, 7949 (2008).
- ³³ K. Miyoshi, E. Kojima, S. Ogawa, Y. Shimojo, and J. Takeuchi, *Physical Review B* **87**, 235111 (2013).
- ³⁴ F. Kretzschmar, B. Muschler, T. Böhm, A. Baum, R. Hackl, H.-H. Wen, V. Tsurkan, J. Deisenhofer, and A. Loidl, *Physical Review Letters* **110**, 187002 (2013).
- ³⁵ C. Liu, T. Kondo, R. M. Fernandes, A. D. Palczewski, E. D. Mun, N. Ni, A. N. Thaler, A. Bostwick, E. Rotenberg, J. Schmalian, S. L. Bud'ko, P. C. Canfield, and A. Kaminski, *Nature Physics* **6**, 419 (2010).
- ³⁶ V. G. Kogan and R. Prozorov, *Reports on Progress in Physics* **75**, 114502 (2012).
- ³⁷ R. Thomale, C. Platt, W. Hanke, J. Hu, and B. A. Bernevig, *Physical Review Letters* **107**, 117001 (2011).